Supplementary Information

Solvent preparation

The solvent TEGDME (Aldrich) is first soaked over a piece of Li metal for 10 hours to remove moisture. It is then distilled under vacuum and stored under Ar atmosphere until use. The activated carbon (AC) powders in this work are moisture sensitive. When the AC powders are not freshly prepared, they are further heated at 250°C under vacuum to remove internally adsorbed moisture before use.

Porosity of the activated carbon

Nitrogen adsorption/desorption isotherm measurements are carried out to characterize the surface area and porosity of the prepared AC powders. The N_2 adsorption isotherm and the pore size distribution are shown in Figure S1. The N_2 adsorption isotherm of the AC shows a type I curve with a H4 hysteresis loop according to the IUPAC classification. The amount of adsorbed nitrogen increases quickly below 0.01 P/P_0 (relative pressure) as shown in the magnified view in the inset, which indicates that the AC contains large amounts of micropores (<2 nm). The hysteresis in the middle pressure range suggests the existence of mesopores. The size in the hysteresis loop is related to the mesopore volume and the connectivity of the pores. Figure S1 b shows the variation of pore size distribution evaluated by density function theory and the two dominant peaks are observed. One peak locates at ~1 nm and the other is ~ 3 nm that are consistent with the result shown in Figure S1 a. The pore volume and surface area of the AC are 2.4 cm^3/g and 3838 m^2/g, respectively.

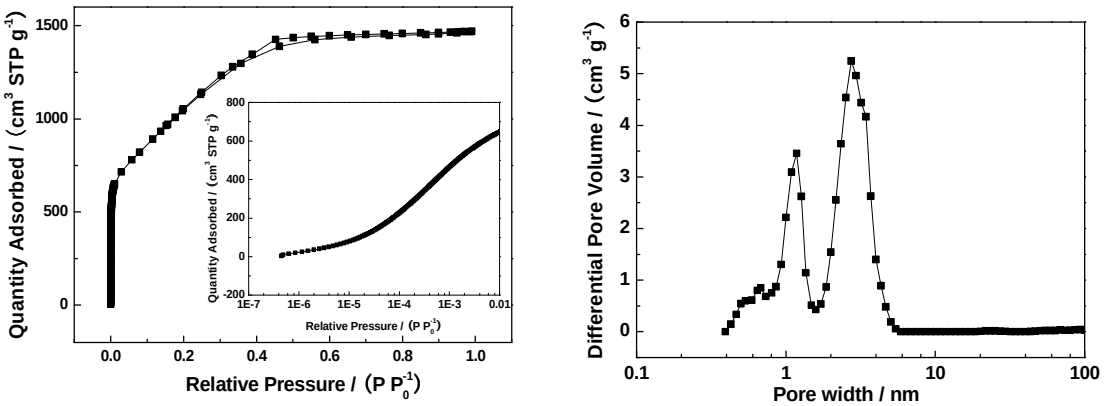

(a) (b)

Figure S1 (a) Nitrogen adsorption/desorption isotherms at 77 K; (b) Pore size distribution of AC by density function theory

Elemental analysis of the activated carbon

Table 1 shows elemental analysis of the activated carbon by X-ray fluorescence (XRF) spectrometer. This activated carbon possesses negligible amounts of Ni and V, but has potassium and calcium in the range of 1410 and 1170 ppm. The results show that this super activated carbon does not possesses high content of transitional metal. The activated carbon that has been treated with acid removes all elements except K and a small amount of Cr as shown in Table 1. The acid treated AC gives a similar cell performance as the untreated AC.

Table 1 Elemental analysis of the activated carbon by X-ray fluorescence (XRF) spectrometer. Also give is the elemental analysis of an acid treated sample.

Element	Amount (ppm)	Amount (acid treated sample) (ppm)
K	1410	1740
Si	444	125
Ca	1170	82.9
Cr	262	211
Fe	486	205
Ni	83.1	16.2
S	12.6	12.7
V	6.12	0
Mn	31	0
Co	7.85	0
Cu	22.5	27.5
Zn	12.1	15.2
Sr	49.1	0
Cl	100	181
C	995000	99700

Cycling data

Figure S2 shows the cycling profile at 0.1 mA cm^{-2} with a discharge capacity of 1000 mA h g^{-1} obtained by controlling the discharge time. The charged capacity starts to fade after the first cycle, probably due to electrolyte decomposition.

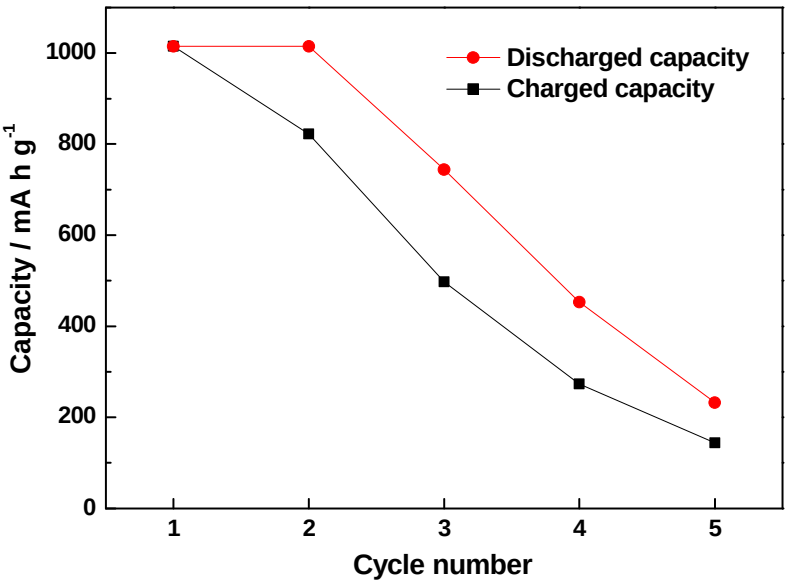

Figure S2. Variation of discharged and charged capacity on the number of cycles

Additional SEM images

The size of the AC particles ranges from a few to tens of μm, as shown in Figure S3a. After discharge the toroidal particles grow on the surface and edges of AC particles with different size asshown in Figure S3b.

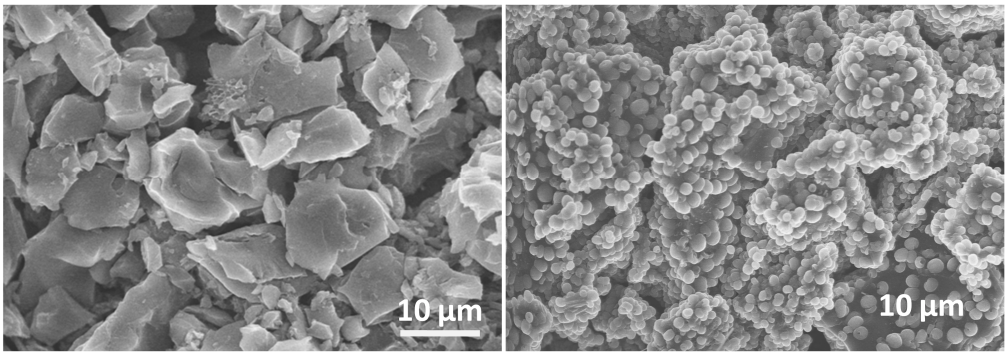

(a) (b)

Figure S3 (a) the pristine activated carbon surface, (b) after discharge with 1000 mA h/g

Simulation techniques:

In this work, two density functional methods were used. The first is the DFT planewaves method that implemented in the Vienna Ab Initio Simulation Package, which based on PBE functional spin polarized calculations. For the planewaves calculations, the projector augmented wave (PAW) method was used to represent the interaction between the core electrons and valence

electrons, and the Kohn-Sham valence states (*2s* for Li, *2s2p* for O) were expanded in plane wave basis sets up to a kinetic energy cutoff of 400 eV. This method was used to compute LiO_2 crystal solid, Li_2O_2 crystal solid and its surfaces.[1] The second is the B3LYP density functional method that based on the 6-31G(d) Gaussian-type basis set as implemented in the Gaussian09 code. This method was used to compute all the Raman spectra intensity of the LiO_2, Li_2O molecule, and $(Li_2O_2)_n$ clusters with n = 1-4, 16.[2]

Oxygen oxidation state and its correlation with vibrational frequencies from DFT:
When the O-O stretching frequencies of DFT values are plotted against the oxidation state of the oxygen atom for O_2, LiO_2, and Li_2O_2, a linear correlation is observed as indicated in Figure S4. This is simply because as O_2 is reduced, the additional electrons occupy the π* antibonding orbitals of the O_2 molecule. Due to charge transfer from the lithium ions, the superoxide anionic oxygen species has one more electron in a π*-level, and its spin configuration is S=1/2 which yields the oxidation state ~ -1.0*e* for an O_2 unit that forms a superoxide (O_2^-). For the peroxide ion, the one extra electron fills up the π*-level, and causes its spin moment to vanish (S=0) and yields the oxidation state ~ -2.0 e (O_2^{2-}). Thus, due to the simple electrostatic interaction from the extra electron in the π*-orbital, the O-O bond strength is weakened and its stretching frequency goes down as the oxidation state of oxygen is increased. The extra electron in the π*-orbital results in a larger *O-O* bond distance, e.g. 1.21 Å (O_2 neutral), ~ 1.35 Å (O_2^- superoxide species), and ~ 1.56 Å (O_2^{2-} peroxide species).

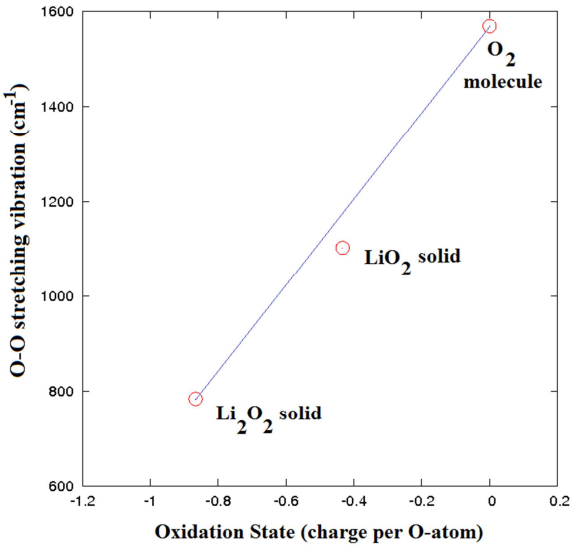

Fig. S4: The computed O-O stretching vibrational frequencies of Li_2O_2, LiO_2 solid, and O_2 molecule based on VASP PBE planewave calculations. The oxidation state of individual O-atom is predicted based on Bader charge partition scheme.

DFT evidence for unsaturated spins
In order to understand the presence of spins in the discharge product from Li-O_2 cell, we used DFT calculations to explore the possibility of magnetism present on the Li_2O_2 surfaces. Instead of being exclusively dominated by peroxide species, we found that the presence of superoxide species with spins appears to be an important factor that yields the magnetic state solution to

these $(Li_2O_2)_n$ stoichiometric surfaces and clusters. Based on our previous study in Li_2O, Li_2O_2 and LiO_2 crystalline solid[5], we constructed a few possible low index stoichiometric surfaces of Li_2O_2 and studied their electronic properties. Given that the Li_2O_2 crystal is expected to be a bulk insulator[3-5], our DFT calculations predict that the electronic properties of the majority of the stoichiometric Li_2O_2 surfaces are surprisingly distinctive from its Li_2O_2 crystalline solid. From the low index stoichiometric surfaces of Li_2O_2, we found only the non-metallic [110] surface prefers a non-magnetic state (i.e. non-spin polarized solution), while the remaining surfaces (i.e. [100], [001], [1-10], [111], [1-11]) prefer a magnetic state, i.e. S = ½ and 1 spin polarized solution with finite magnetization (Fig. S5). For these spin polarized stoichiometric surfaces, the magnetic spin states (spin polarized solution) are overall found to be energetically favorable over the non-magnetic state (non-spin polarized solution) within a range of 0.11 to 0.36 eV. As shown in Fig. S5, these spin polarized stoichiometric surfaces are predicted to be metallic-like and conductive with a finite density of state (DOS) cross the Fermi level (E_f), similar to the metallic feature of the oxygen rich Li_2O_2 surfaces (e.g. O-rich [001] surface) predicted recently[6]. From the site projected DOS in Fig. S5, the metallic states crossing E_f are mostly attributed to the surface bounded oxygen species with the presence of spin magnetization (Fig. S5). Through the charge partition scheme based on Bader charge analysis, the oxidation state (i.e. charge per-O atom or an O_2-dimer) of oxygen species can be determined. We found the majority of these surface bound oxygen species with finite spin magnetization are predicted to be a "superoxide"-like oxygen ions (O_2^-), whereas the subsurface oxygen ions that with negligible spin magnetization (Fig. S5) are predicted to be the conventional non-magnetic "peroxide"-like oxygen ions (O_2^{2-}). Similar features can also found in some O-rich Li_2O_2 surfaces as shown in Fig. S6. Thus this confirms the observation of spins from our experimental SQUID measurement on Li_2O_2 discharge product.

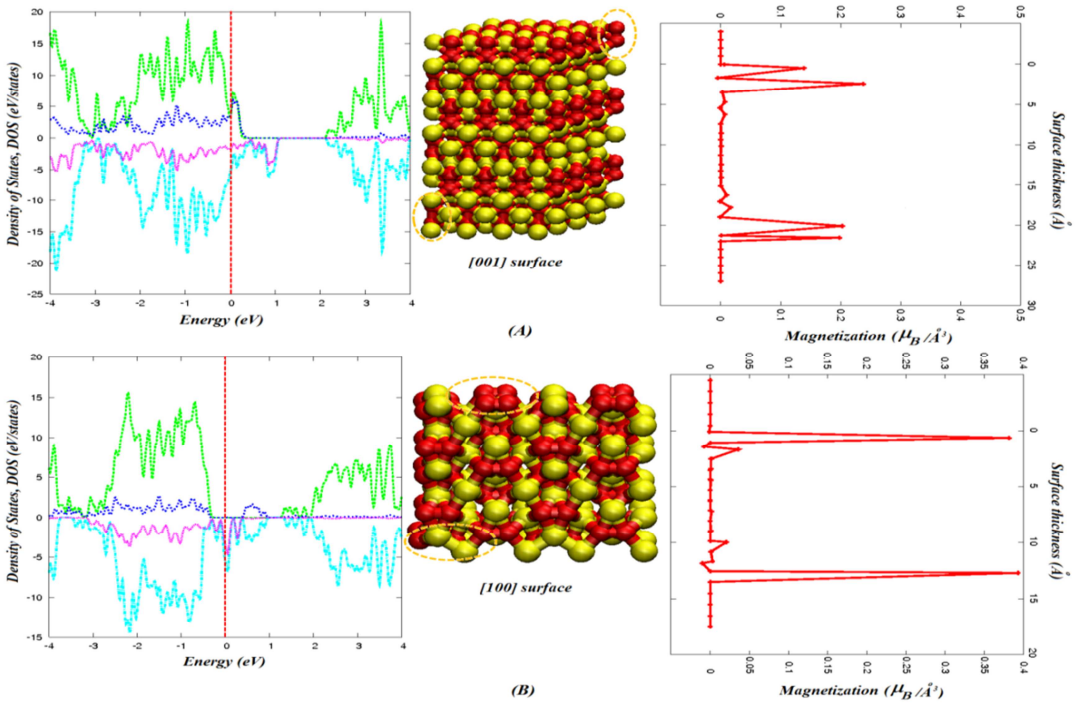

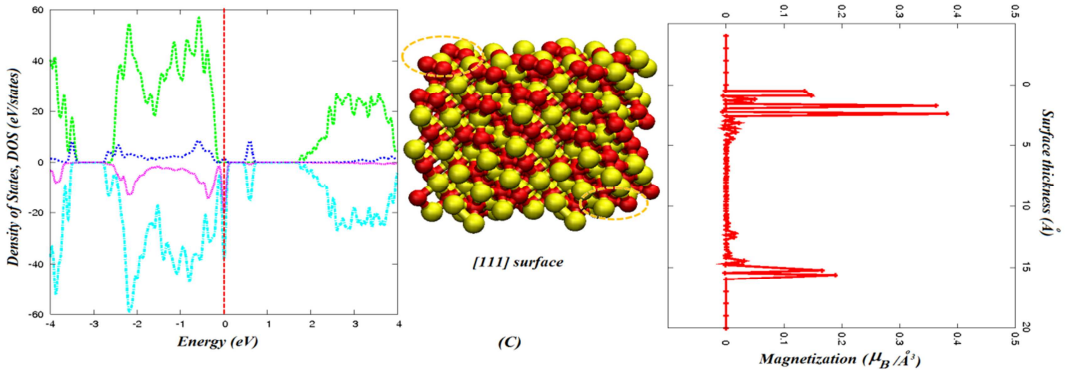

Fig. S5: The calculated spin density of states (DOS) (i.e. spin up and spin down) and site projected magnetization of the few selected low index stoichiometric Li_2O_2 surfaces that prefers high spin states: (a) [001] (b) [100] (c) [111] surface. In the magnetization plot (right), the vertical axis represents the atomic position along the surface thickness, i.e. the top surface atoms appear at the top close to zero. The circled atoms represent the surface bound superoxide-like species which have large magnetization and finite DOS cross the Fermi level (i.e. at zero in red lines).

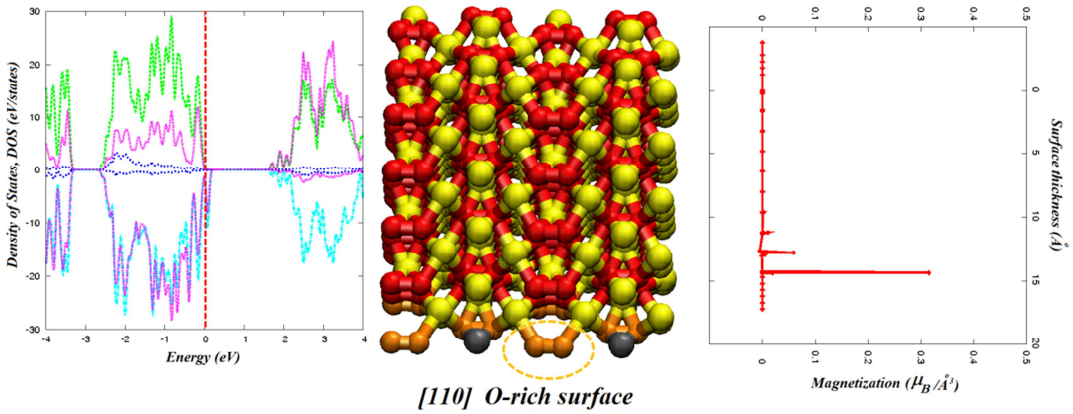

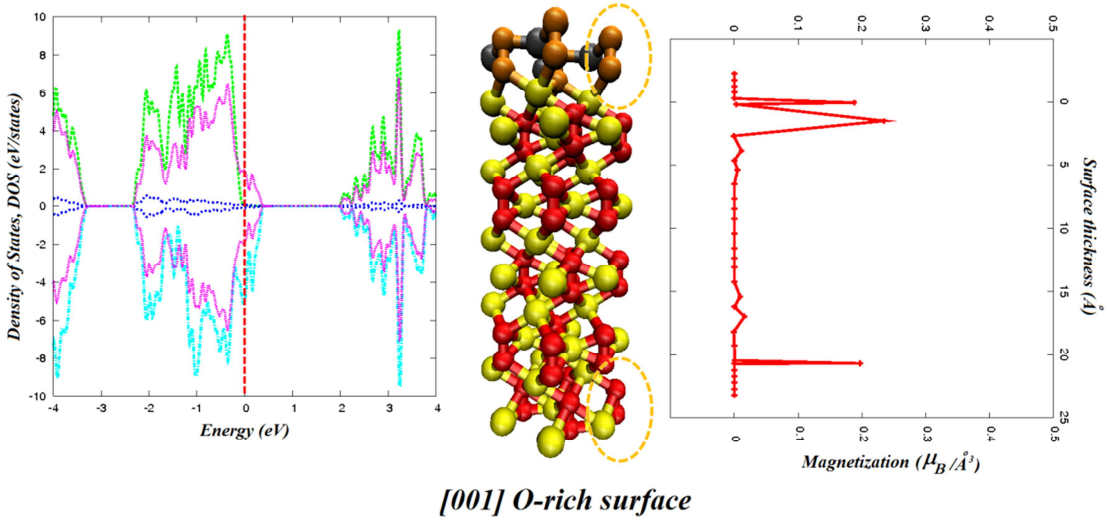

Fig. S6: The calculated spin density of states (DOS) (i.e. spin up and spin down) and site projected magnetization of a few selected low index O-rich Li_2O_2 surfaces that prefer high spin states: (top) [110] O-rich surface (bottom) [001] O-rich surface. In the magnetization plot (right), the vertical axis represents the atomic position along the surface thickness, i.e. the top surface atoms appear at the top close to zero. The circled atoms represent the surface bound superoxide-like species that have large magnetization and finite DOS crossing the Fermi level (i.e. at zero in red lines). The O-rich layer is shown with Li^- (gray in color) and O^- (orange in color) atom.

References

1. Lau, K. C.; Curtiss, L. A.; Greeley, J. *Journal of Physical Chemistry C* **2011,** 115, (47), 23625-23633.

2. Lau, K. C.; Assary, R. S.; Redfern, P. C.; Greeley, J. P.; Curtiss, L. A. *The Journal of Physical Chemistry C* **2012** DOI: 10.1021/jp306024f.

3. Mo, Y.; Ong, S.P.; Ceder, G. *Phys. Rev. B*, **2011**, 84, 205446.

4. Hummelshoj, J. S.; Blomqvist, J.; Datta, S.; Vegge, T.; Rossmeisl, J.; Thygesen, K. S.; Luntz, A. C.; Jacobsen, K. W.; Norskov, J. K. *J. Chem. Phys.* **2010**, 132, 071101−4.

5. Garcia2011, Garcia-Lastra, J. M.; Bass, J. D.; Thygesen, K. S. *J. Chem. Phys.* **2011**, 135, 121101

6. Radin, M. D.; Rodriguez, J. F.; Tian, F.; Siegel, D. J. *J. Am. Chem. Soc.* **2012**, 134, 1093−1103.